Influence of stacking faults in polymorphic ZnS on the d^5 crystal-field states of Mn^{2+}

U. W. Pohl, A. Ostermeier, W. Busse, and H.-E. Gumlich
Institut für Festkörperphysik, Technische Universität Berlin, Hardenbergstrasse 36, D-1000 Berlin 12, West Germany

(Received 10 April 1990; revised manuscript received 18 June 1990)

In polymorphic ZnS:Mn novel luminescence centers attributed to Mn^{2+} in axial crystal fields have been detected with use of site-selection spectroscopy. The shift of the zero-photon lines with respect to the cubic Mn^{2+} center within the three excited levels $^4T_1(G)$, $^4T_2(G)$, and $^4E(G)$ and the observed fine structures fit well into the findings of Mn^{2+} centers in stacking-faulted ZnS which have been reported earlier. The overall picture is completed by the detection of the excitation energies within the $^4T_2(G)$ level of all observed Mn^{2+} centers. A general crystallographic scheme is presented to classify lattice sites with different sequences of stacking layers up to the second next Zn-S layer with respect to the impurity. Based on the lattice classification, a superposition principle is proposed which describes the effect of several lattice distortions upon the $3d$ transitions of Mn^{2+} on different lattice sites. The structural considerations lead to assignments of all Mn^{2+} luminescence centers to specific lattice sites, which are in good agreement with the findings in the spectra of other transition-metal impurities in stacking-faulted ZnS.

I. INTRODUCTION

Zinc sulfide can grow in different modifications. Besides the cubic zinc-blende and the hexagonal wurtzite structures, polymorphic structures occur. Substitutional impurities as transition metals (TM's) can thus be incorporated at different lattice sites. The energies of transitions within the d shell of TM impurities depend on the adjacent lattice environment, and thus various axial centers appear in optical spectra of polymorphic ZnS in addition to the cubic center.

All modifications of ZnS consist of sequences of hexagonal Zn-S layers being stacked along the direction of growth ([111] for cubic, [00.1] for hexagonal structure). There exist three equivalent layers (A, B, and C) which determine the crystal structure by the stacking sequence (for example, ABC for cubic, AB for wurtzite structure). TM impurities substituting Zn^{2+} ions are located in a tetrahedrally coordinated S^{2-} environment which belongs to two Zn-S layers. Thus, four different lattice sites exist for a substitutional impurity if the Zn-S layers above and below these two layers are considered. The four sites are referred to as AN (cubic, zinc blende), AS, PN (axial distorted), and PS (hexagonal, wurtzite).[1] (In the notation of Buch *et al.*,[1] "P" and "A" refer, respectively, to prismatic and antiprismatic, while S indicates the presence of a single-axial third neighbor, and N its absence.)

The Mn^{2+} ion, in particular, is a sensitive probe for studying the influence of the lattice environment on TM energy levels, because the five d^5 absorption bands in ZnS which show a pronounced fine structure[2] are also excitation bands[2,3] of the Mn^{2+} luminescence. Thus, site-selection spectroscopy can be applied to detect even weak zero-phonon lines, which, in absorption spectra, often are hidden by stronger transitions of other centers.

The effect of the stacking order of the Zn-S layers above and below the two layers containing the Mn^{2+} impurity on the internal d transitions has been reported by several authors.[4–6] The theoretical description,[4] however, is not yet given in a satisfactory way. Magnitude and order of the observed energy shifts of zero-phonon lines (ZPL's) due to different Mn^{2+} centers are not described correctly. Also, the prediction that no influence of the stacking sequence of layers beyond the four layers considered above exists[1,4] does not hold. In transitions of Mn^{2+} involving the $^4T_1(G)$ and $^4E(G)$ levels the effect of the sequence of two further stacking layers has been demonstrated.[7,8]

In the present paper the influence of the stacking sequence of these additional layers could also be detected within the Mn^{2+} excitation spectra to the $^4T_2(G)$ level. Completed by the detection of three further axial distorted Mn^{2+} centers, now an almost complete survey of all luminescence centers which are possible under consideration of six Zn-S layers can be given. The transition energies of all axial distorted Mn^{2+} centers are shifted to higher energies with respect to the corresponding transitions of the cubic center. As it turned out, a pattern of transition-energy shifts induced by stacking faults (SF's) could be observed. All energy shifts were found to be characteristic for different stacking sequences of layers nearest and, also, second-nearest to the two Zn-S layers containing the Mn^{2+} impurity.

The energy-shift pattern leads to a superposition principle which describes the influence of SF's on the TM energy levels as a sum of crystal fields induced by the stacking layers. Therefore, a classification scheme of all 16 lattice sites that are possible within the range of six Zn-S layers will be given. This classification leads to assignments of all lines in the optical spectra to specific lattice sites with different stacking orders. These assignments are in accordance with the fine structures of the zero-phonon lines and supported by the effects of SF's on the energy levels of other TM impurities.

II. CRYSTALLOGRAPHIC CLASSIFICATION

Our motivation to look for further, as yet unobserved axial centers arises from considerations of possible stacking-layer sequences. Five axial distorted Mn^{2+} centers have been reported earlier in addition to the four centers AN, AS, PN and PS.[7] Three of these centers appear only slightly shifted with respect to the cubic center AN and an additional center next to each of both centers AS and PN. From the assignments of these supplementary axial distorted centers to Mn^{2+} ions at lattice sites which differ in the stacking sequence beyond the four layers next to the impurity, we conclude that a certain number of additional centers are expected to exist, since, as from crystallographic aspects, a total number of 16 lattice sites is possible if one considers a lattice range including two layers in addition to the four layers containing the impurity.

A survey of all 16 inequivalent lattice sites that are possible within the range of six Zn-S layers is given in Fig. 1. The stacking sequences are drawn in the $(\bar{1}01)$ plane of the cubic lattice [which corresponds to the (11.0) plane of the wurtzite lattice]. They are arranged according to the four main lattice sites AN, AS, PN, and PS, which differ only in the lattice environment next to the impurity. If above and below the four Zn-S layers containing the impurity one further layer is taken into account, each of the four main lattice sites has four possible "subsites." The number of SF's increases going from AN (the stable cubic phase of ZnS) to PS. In this arrangement the hexagonal wurtzite phase corresponds to the site PS3 consisting completely of SF's.

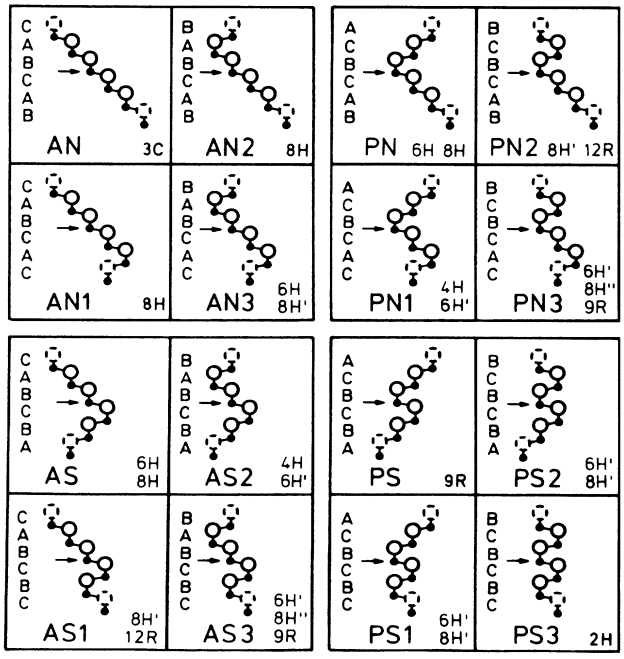

FIG. 1. Lattice-classification scheme of all 16 possible stacking sequences within a range of six Zn-S layers, drawn in the (11.0) plane. Zn^{2+} and S^{2-} ions are represented by points and circles, respectively; the position of the impurity is marked by an arrow. The letters *ABC* on the left-hand side denote Zn-S layers. The lattice structures in each of the figures are those which contain the displayed stacking sequences. Inequivalent structures are marked by quotation marks: $6H$:(3,3), $6H'$:(2,2,1,1), $8H$:(4,4), $8H'$:(3,3,1,1), $8H''$:$(2,1,1)_2$, $9R$:$(2,1)_3$, and $12R$:$(3,1)_3$.

The assignments of the cubic center to the AN site and the hexagonal center to the PS3 site is reliable because purely cubic and purely hexagonal samples, checked by x-ray analysis, only show the corresponding ZPL's both in the emission and excitation spectra.[4,9] The assignments of the two additionally observed main centers to the axial sites AS and PN, however, are not unequivocal. Both sites have axial symmetry and should occur in equal abundance because one SF creates both an AS and a PN site; see Fig. 1. By use of optically detected magnetic resonance (ODMR) a correspondence of the two axial Mn^{2+} centers observed in optical spectra to the two axial Mn^{2+} centers observed in EPR (Ref. 1) has been established.[10] A safe assignment of the two centers, each to a definite site of either AS or PN, however, could not be given.[1,10] A similar problem arises in the attribution of the centers which differ in the stacking order of the two outer layers of the six Zn-S layers. Therefore, in the present paper the observed centers are labeled ax1, ax1,1, etc., and a possible attribution of these labels to lattice sites as AS, AS1, etc. will be discussed in Sec. IV.

The crystal structures given in the classification scheme depicted in Fig. 1, which contains the displayed stacking sequences, each evoke only specific lattice sites for a substitutional impurity. From these considerations, some centers are always expected to appear simultaneously. Thus, in the case of a hexagonal $4H$ structure, only centers connected to the sites PN1 and AS2 should appear.

III. EXPERIMENTAL RESULTS

Polymorphic $Zn_{1-x}Mn_xS$ crystals doped with low amounts of Mn (x_{Mn} is typically of order 10^{-4}) which have narrow ZPL's have been investigated. The stacking-faulted structures were found to vary along the direction of growth. We thus selected—spatially—the interesting areas within the samples. The luminescence was excited by an excimer-laser-pumped dye laser ($\Delta\tilde{\nu}\approx 0.6\ cm^{-1}$) at temperatures between 1.9 and 15 K.

For the search of as yet unobserved centers, a careful selection of suitable ZnS:Mn samples was evident. The appearance of centers connected to the PS site which normally have little abundance in polymorphic samples has been taken as a criterion. In many cases the search for weak centers could be facilitated by recording the spectra at $T \leq 2$ K due to the suppression of thermalized-emission ZPL's. As a helpful tool, Voigt-curve analysis by χ^2 fits assuming square-root error of the intensity was applied for the determination of energy, intensity, and full width at half maximum (FWHM) of weak ZPL's on which are superimposed stronger lines of other centers. For all ZPL's the Voigt profile[11] turned out to be the only suitable analytic representation. The technique of

contour-line plotting described earlier[7] was used to resolve weak transitions. The typical fine-structure pattern of the ZPL's allows the recognition of coherent groups even if they are superimposed on more intensive structures.

A. Search for axial centers

On the basis of the crystallographic classification of impurity sites presented in Sec. II, the experimental tools have been applied to detect further, as yet unobserved centers. In the case of the cubic center AN, three supplementary centers have already been reported.[7] Therefore, our main interest was the search of additional luminescence centers near the two axial centers and the hexagonal center. In order to achieve good site selection, we focused our attention on the pronounced zero-phonon lines of the Mn^{2+} transitions involving the $^4T_1(G)$, $^4T_2(G)$, and $^4E(G)$ states. The origin of the observed fine structure is well known for the Mn^{2+} in a cubic environment. The energy scheme of these levels and the selected transitions are shown in Fig. 2. The energy levels observed for an axial distorted center which is created by stacking faults has been added.

Groups of ZPL's near the center axial 1 (ax1), which is referred to as AS in Refs. 4 and 7, are shown in Fig. 3. The spectra are given in form of a contour-line diagram of a series of 22 excitation spectra of the $^4E(G)$ level. The emission energies were varied in steps of 1 cm^{-1}. In this diagram coherent groups of ZPL's referring to one center, e.g., two ZPL's in emission and three ZPL's in excitation, are connected by lines. Two distinct centers, ax1 and ax1,1, can be recognized. The positions of two further weak centers, ax1,2 and ax1,3, can be be determined by Voigt-curve analysis. The corresponding energies of the χ^2 fits are marked in Fig. 3. Besides the center ax1, only the center ax1,2 has been reported until now (AS2 in Ref. 7) within the spectral range shown in Fig. 3.

Within the spatially selected crystal range used in the spectra of Fig. 3, the center ax1,1 is dominating. Simultaneously, in the spectral range of the center ax2 (referred

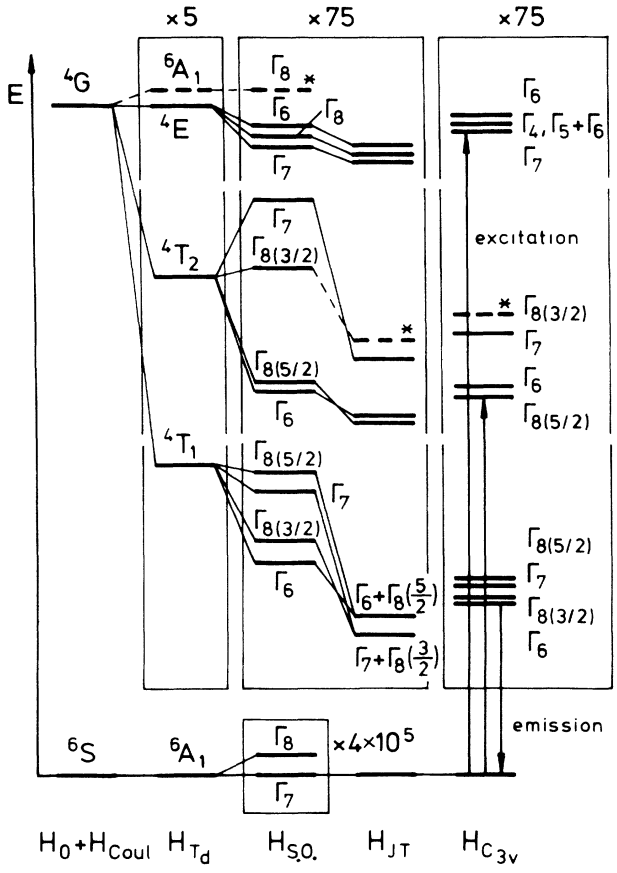

FIG. 2. Energy-level scheme of the Mn^{2+} ion. In cubic ZnS the optical fine structure is described by the interaction of the free-ion levels given by H_0+H_{Coul} with the crystal-field interaction H_{T_d} and the spin-orbit interaction $H_{s.o.}$ reduced by the Jahn-Teller interaction H_{JT}. Stacking faults evoke additional crystal fields of axial C_{3v} point-group symmetry. The displayed distorted-term scheme refers to ax2 and hex centers. The arrows denote transitions of excitation and emission spectra. Transitions to dashed levels marked by an asterisk are forbidden.

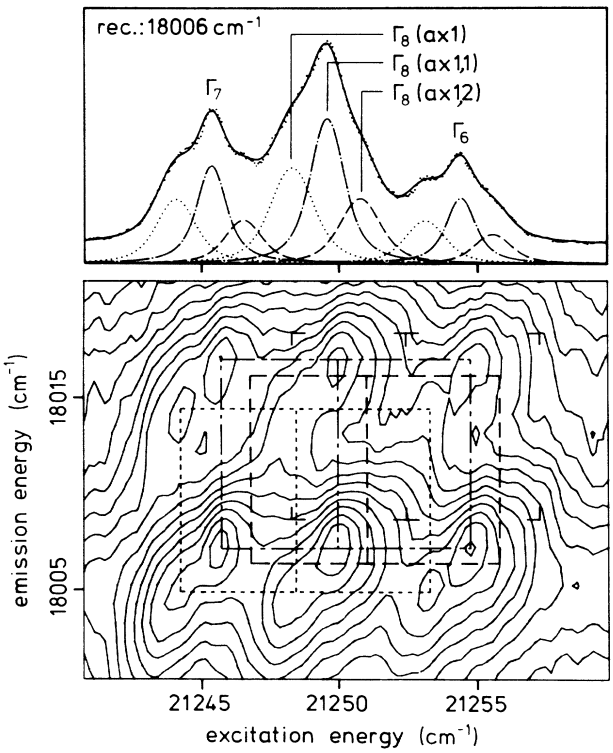

FIG. 3. Countour-line diagram of isointensities of combined $^4T_1(G)\rightarrow{}^6A_1(S)$ emission and $^6A_1(S)\rightarrow{}^4E(G)$ excitation spectra of the ax1 centers in stacking-faulted ZnS:Mn at $T=5$ K. The intensities are given on a logarithmic scale, i.e., the intensities change by a constant factor going from one contour line to the next. Coherent groups of ZPL's are connected by lines: $\cdots$, ax1; $-\cdot-\cdot-\cdot$, ax1,1; $-\ -\ -$, ax1,2; for ax1,3 only the energies of fit positions are marked. The separate excitation spectrum shown at the top is recorded at an emission energy of 18 006 cm^{-1}. At this emission energy the weak center ax1,2 can be recognized, as can the dominating centers ax1,1 and ax1.

to as PN in Ref. 4 and 7) a strong center denoted ax2,2 appears: see Fig. 4. Both novel centers ax1,1 and ax2,2 are more intensive than the centers ax1 and ax2, which usually dominate in stacking-faulted ZnS:Mn. They are also much stronger than the already known centers ax1,2 (AS2 in Ref. 7) and ax2,1 (PN1 in Ref. 7, SF4 in Ref. 8). The spectra have been recorded at $T=2$ K to avoid overlapping with thermalized lines (see Sec. III C). Nevertheless, some weak thermalized-emission ZPL's are observed. The search for a fourth center in the case of ax2 centers was not successful.

The ZPL's due to hexagonal centers have been found to be very weak within most of the polymorphic samples. No safe detection of supplementary hexagonal centers has been achieved so far.

B. Excitation levels within the $^4T_2(G)$ state

While the excitation levels of the four main centers cub, ax1, ax2, and hex within the $^4T_2(G)$ are known,[7] no data exist in the case of the supplementary centers. In order to provide this valuable information on the effect of SF's on TM energy levels, the corresponding excitation ZPL's have been recorded for all observed centers. The results of the excitation measurements on the $^4T_2(G)$ level are summarized in Fig. 5, including the results described in the preceding subsection. For clarity, only the energy shifts of the strongest ZPL's corresponding to the selected centers with respect to the main centers have been drawn.

The energy shifts of all optical centers observed within the $^4T_2(G)$ excitation spectra exhibit a symmetry with respect to an average energy. The symmetric pattern is also observed within the $^4T_1(G)$ and $^4E(G)$ levels.

C. Zero-phonon-line fine structure

In the preceding subsection only the energy shift of each ZPL group with respect to the ZPL's of the cubic center has been considered. The effect of the SF's on the TM d-electron spin-orbit splitting provides further information on the type of interaction.

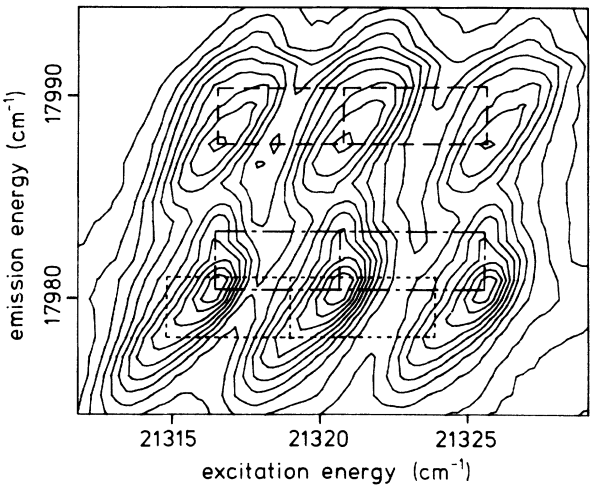

FIG. 4. Contour-line diagram of the $^4T_1(G)\rightarrow{}^6A_1(S)$ emission and $^6A_1(S)\rightarrow{}^4E(G)$ excitation of the ax2 centers recorded at $T=2$ K on a logarithmic intensity scale. Line types: $\cdots$, ax2; $-\cdot-\cdot-\cdot$, ax2,2; $-\ -\ -$, ax2,1.

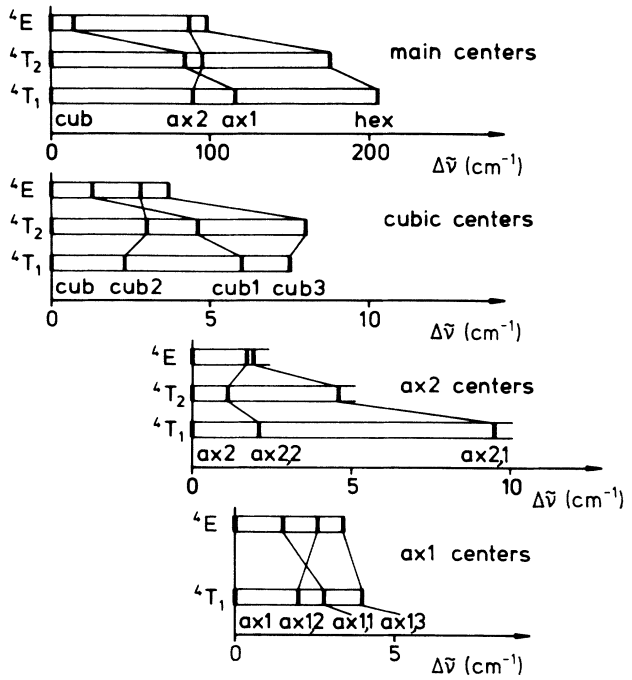

FIG. 5. Relative energy shifts of the centers of gravity of the ZPL's connected to different Mn^{2+} centers in stacking-faulted ZnS. The energies of the following transitions have been taken as references: $\Gamma_7+\Gamma_{8(3/2)}$ ($^4T_1(G)$) for cub and ax1, $\Gamma_6(^4T_1(G))$ for ax2 and hex, and $\Gamma_{8(5/2)}(^4T_2(G))$ and $\Gamma_8(^4E(G))$—which corresponds to $\Gamma_4,\Gamma_5+\Gamma_6(^4E(G))$—for axial distorted centers.

The emission ZPL fine structure of the four main centers is shown in Fig. 6. The energies of all lines have been determined by Voigt-curve analysis and are listed in Table I. The fine structure of the emission ZPL's connected to the main centers cub, ax1, and ax2 are well known[5,8] and understood within the framework of the Jahn-Teller effect.[12,13] Owing to good site selection, the fine structure of the center hex can now be presented almost without interfering with emissions of other eventual hex centers. This allows the recognition of the lowest excited state and the correction of the fine-structure splittings reported earlier.[7]

In the case of center ax2, Voigt-curve analysis revealed for the first time a slight splitting of the two lines starting from Γ_8 states (Table I), which have been shown earlier to split in two under uniaxial pressure.[8,13]

The intensity ratios of the emission lines observed at very low temperatures to their corresponding thermalized emissions (Fig. 6) are well described by Boltzmann weighting factors if the degree of degeneracy (Γ_6 and Γ_7 twofold, Γ_8 fourfold) and the transition probabilities [taken from $^4T_1(G)$ excitation spectra[14]] of the involved states are taken into account. For centers cub and ax1 the experimental results agree well with the calculations of the relative dipole strength (RDS).[8] Some discrepan-

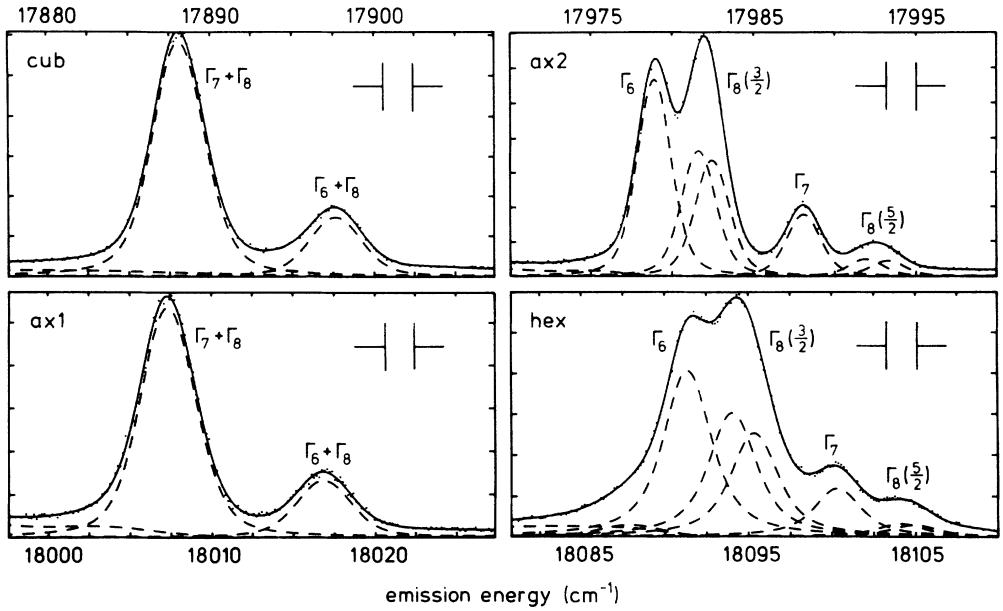

FIG. 6. Emission zero-phonon-line fine structure due to the transition $^4T_1(G) \rightarrow {}^6A_1(S)$ of the four main Mn^{2+} centers in stacking-faulted ZnS recorded at $T=8$ K. Dotted line, experimental values; dashed, Voigt-analysis curves; solid, sum of Voigt curves.

TABLE I. Energies of zero-phonon lines, W, due to different Mn^{2+} centers in stacking-faulted ZnS. The strongest line within each electronic level is taken as a reference for other lines of the same level. The temperature-dependent fine-structure splittings of the $^4T_1(G)$ level are given for $T=8$ K. The relative shifts of the strongest ZPL's of the stacking-faulted centers, dW, refer to the energy of the cubic center "cub" at the AN site.

	$^6A_1(S) \rightarrow {}^4E(G)$ (cm^{-1})				$^6A_1(S) \rightarrow {}^4T_2(G)$ (cm^{-1})			$^4T_1(G) \rightarrow {}^6A_1(S)$ (cm^{-1})			
	dW	W			dW	W		dW	W		
	(±0.2)	Γ_8	Γ_7	Γ_6	(±0.2)	$\Gamma_{8(5/2)}$	Γ_6	(±0.5)	$\Gamma_7+\Gamma_{8(3/2)}$	$\Gamma_6+\Gamma_{8(5/2)}$	
cub	0	21 235	−4.3	+4.9	0	19 680	+4.0	0	17 889	+9.5	
cub1	+1.3	21 236	−4.4	+4.9	+4.6	19 685	+4.0	+6.0	17 895	a	
cub2	+2.8	21 238	−4.3	+4.9	+3	19 683	+4	+2.3	17 891	a	
cub3	+3.7	21 239	−4.4	+4.8	+8	19 688	+4	+7.5	17 896		
ax1	+13.8	21 249	−4.3	+4.9	+84	19 764	+3(?)	+116.0	18 005	+9.5	
ax1,1	+15.3	21 250	−4.2	+4.8				+118.8	18 008	a	
ax1,2	+16.4	21 251	−4.3	+4.9				+118	18 007	a	
ax1,3	+17.2	21 252	−4.3	+4.9				+120	18 009		
									W		
									Γ_6	$\Gamma_{8(3/2)}$	Γ_7	$\Gamma_{8(5/2)}$
ax2	+86.5	21 319	−4.2	+4.9	+94.8	19 775	+5.9	+88.9	17 978	+3.1	+9.2	+13.7
ax2,1	+88.4	21 321	−4.2	+4.9	+99.4	19 780	+4.8	+98.4	17 988	a	a	a
ax2,2	+88.2	21 321	−4.2	+4.9	+95.9	19 776	+6.8	+91.0	17 980	a	a	a
ax2,x	b				+98.6	19 779	+4.1	+91.0	17 980	b	b	b
hex	+98	21 331	−4.2	+4.8	+175	19 855		+205	18 098	+3.3	+9.0	+13.2

[a] Identical emission ZPL fine structure within the limit of error.
[b] Center ax2,x (see text).

cies, however, must be mentioned in the case of the ax2 emission lines. The observed splittings of the Γ_8 lines which (in contrast to Γ_6 and Γ_7 lines) can be induced by axial fields show that the four emission lines of the center ax2 have to be attributed to the terms Γ_6, $\Gamma_{8(3/2)}$, Γ_7, and $\Gamma_{8(5/2)}$, respectively, with increasing energy. This order of the terms is described by a Huang-Rhys factor S of the order of 0.5, rather than the value $S \approx 1.4$ given earlier.[8] Also, the RDS ratios of the four lines, found to be approximately 1:(1+1):1:(0.5+0.5), deviate from the computed values.[8]

The ZPL structures of the cub- and ax1-center emissions are identical. Within the limits of accuracy, our measurements also revealed that the emission fine structure of centers ax2 and hex are essentially identical. Between a main center and the corresponding supplementary centers only negligible differences of the emission ZPL fine structures have been observed.

Within the excitation ZPL fine structure of the $^4T_2(G)$ level, some differences have been found for the ax2 centers. Based on the calculation of the relative dipole strength of the transitions to the two states $\Gamma_6(^4T_2)$ and $\Gamma_{8(5/2)}(^4T_2)$ and their Jahn-Teller reduced spin-orbit splitting,[8] a safe attribution of ZPL's to the centers ax2, ax2,1, and a likely assignment to ax2,2 can be given. In the case of ax2,2, the interference with another center, denoted as2,x, which has the same emission energy as center ax2,2, complicates the interpretation of the spectra. Center ax2,x is assumed to belong to the ax2 Mn^{2+} centers because the same thermalization of the emission of this center with respect to the other ax2 centers has been found.

For the ax1 center some indications for the existence of supplementary centers within the $^4T_2(G)$ excitation spectra have been found. Owing to the small spin-orbit splitting and a poor spectral resolution, however, no successful discrimination has been achieved within the $^4T_2(G)$ level.

In the case of the hex center, only one center could be observed.

The $^4E(G)$ excitation ZPL fine structure is almost identical for all observed centers. Some interesting differences, however, have been found within the FWHM of the central $\Gamma_8(^4E(G))$ excitation line. A splitting of this line has been reported only in the case of a crystal exhibiting a perfect wurtzite structure. The splitting into a Γ_4 and a $\Gamma_5+\Gamma_6$ state was found to be 1.2 cm^{-1},[15] a little less than calculated (3 cm^{-1} Ref. 6). In *all* excitation spectra of the ax1, ax2, and hex centers the Γ_8 line was found to have greater FWHM than the Γ_6 and Γ_7 lines. If the identical FWHM of Γ_6 and Γ_7 is taken as a reference, Voigt-curve analysis gives a splitting of the Γ_8 line in these cases. Within a standard deviation of ± 0.1 cm^{-1}, splittings of 0.4 cm^{-1} for the ax1 centers, 0.2 cm^{-1} for the ax2 and ax2,2 centers, 0.5 cm^{-1} for the ax2,1 center, and 0.7 cm^{-1} for the hex center have been obtained. In Table I an average energy has been taken for the $\Gamma_8(^4E(G))$ line. Only the cub centers do not show any $\Gamma_8(^4E(G))$ broadening with respect to the Γ_6 and Γ_7 lines.

IV. DISCUSSION

A. Assignments of the Mn^{2+} centers in polymorphic ZnS

The symmetrical energy-shift pattern of the stacking-faulted Mn^{2+} centers as shown in Fig. 5 is a striking feature for all observed centers in all excited levels. This means the energy of the most strongly shifted center can be described by the sum of the energy of the two corresponding centers with medium energy shifts. As an example, the energy shifts of the center cub3 with respect to cub is approximately given by the sum of the shifts of the centers cub1 and cub2. In principle, this behavior can be understood within the framework of the stacking-layer-sequence classification presented in Sec. II.

As an example, the cubic sites AN and AN3 are considered. The energy of the center cub referring to the AN site is taken as a reference. Site AN1 occurs if one SF below the impurity is present. This SF induces an axial distortion of the cubic potential V_{AN}, say ΔV_{AN1}. In the same way, one SF above the impurity induces ΔV_{AN2}. As shown in Fig. 1, AN3 can essentially be regarded as a combination of the two SF's, AN1 and AN2, being present simultaneously. Thus the relation

$$\Delta V_{AN3} = \Delta V_{AN1} + \Delta V_{AN2} ,$$

i.e., a superposition of the two axial distortions, is expected to be a good approximation. This kind of superposition can be built for all centers summarized in Fig. 5.

Axial terms in the crystal-field potential exclusively cannot explain the energy shifts because, for instance, neither the $^6A_1(S)$ nor the $^4E(G)$ state depend on the crystal-field potential V. The reason is a balance of the effect of the three t_2 and the two e orbitals of the d^5 energy levels with A and E symmetry. Therefore, a splitting parameter Δ describing deviations from this balance has been proposed[4] which should depend on V and on a covalency parameter x. This electronic model has to be completed by a vibronic model as proposed in Ref. 8. Although no complete theoretical description could be given, the findings of the present work show the validity of a superposition model.

On this basis, the center cub3 is assigned to an AN3 site. For any further assignment, an answer to the question of whether center ax1 is connected to an AS site and ax2 to PN or vice versa must be given. From the classification scheme depicted in Fig. 1, the identity of the *nearest* neighborhood of the impurity site of all AN and AS sites, on one hand, and of all PN and PS sites on the other, can be established. Evidently, the influence of the stacking order of the layers nearest the impurity is stronger than the influence of the layers next nearest the impurity. The emission ZPL fine structures shown in Fig. 6 demonstrate similar spin-orbit splittings for the cub and ax1 centers on one hand and for ax2 centers and the hex center on the other. Also, a drastic fine-structure change upon going from ax1 to ax2 is noticed.

At a PN and a PS site the distortion caused by a SF occurs within the first Zn shell surrounding the central

impurity—this means the deviation from the regular stacking order occurs at the second neighbor along the Zn-S-Zn chain displayed in Fig. 1. Thereby, the regular antiprismatic structure of this shell is changed to a prismatic structure, and thus the center of symmetry inversion is removed. In the case of the AS site, the center of inversion is not removed from the first Zn shell. Here the distortion occurs at the third neighbor within a S shell. These structural considerations lead us to the conclusion that the distortion at a PN site should have a stronger influence on the symmetry of the substitutional Mn ion as at a AS site, but with a comparable influence with respect to a PS site. If the Jahn-Teller effect is weakened due to a lower site symmetry, a stronger splitting of the $^4T_1$ state is expected.[12,13] This is in accordance with the observed emission fine structures, Fig. 6. The detection of the hex-center emission ZPL structure shown in Fig. 6 therefore provides a proof of the tentative assignments of ax1 centers to AS sites and ax2 centers to PN sites used by other authors.[4,7]

A similar problem arises in the attribution of the corresponding two supplementary centers with medium energy shift. In this case, however, the spin-orbit splitting of the corresponding pairs of centers is quite similar. We therefore tentatively take the distance of the Mn impurity to the layer with deviating stacking order with respect to the corresponding main center and the observed energy-shift pattern (Fig. 5) as a criterion for the strength of the effect of the SF on the TM energy. This criterion yields the same assignments of the centers ax1 to AS and ax2 to PN as the symmetry considerations discussed in the preceding paragraph.

In the case of the AN sites AN1 and AN2, the deviation from perfect stacking order with respect to the AN site occurs at the AN1 site at the fifth neighbor with respect to the impurity. At the AN2 site the deviation is already encountered within the preceding Zn neighbor—this means the fourth neighbor in the chain. Therefore, the less-shifted center within the $^4E(G)$ level cub1 is attributed to an impurity at the AN1 site and cub2 to an impurity at the AN2 site. In the same way, the assignments of ax1,1 and ax1,2 to sites AS1 and AS2, respectively, are given. Owing to the deviating energy-shift pattern of the medium-shifted ax2 centers, this criterion cannot be applied for further attributions.

A consequence of the lattice-classification scheme (Fig. 1) is the simultaneous appearance of specific sites within a given lattice structure. In Figs. 3 and 4 a crystal spatial range has been selected in which the centers ax1,1 and ax2,2 dominate. In this crystal range the hex center is also observed—with considerable intensity. Considering the lattice classification, this is expected if the crystal contains sequences of two successive SF's which create the sites AS1, PN2, and PS.

The sequence of two SF's seems to be much more likely with an additional layer of normal stacking order between them. This sequence creates 4*H*-structured crystal ranges where solely the sites AS2 and PN1 occur simultaneously. ZnS:Mn samples showing strong 3*C* (cubic) and 4*H* reflexes in Laue-diffraction diagrams, in fact, exhibit dominating ax1,2 and ax2,1 centers. This confirms the attribution of centers ax2,1 and ax1,2 to the lattice sites AS2 and PN1, respectively.

B. Centers of other transition-metal impurities in polymorphic ZnS

Besides Mn^{2+}, several other TM impurity centers have been investigated in polymorphic or polytypic ZnS by other authors. Similar energy-shift patterns as observed in the case of the Mn^{2+} centers (Fig. 5) can be found for other TM centers. A brief summary of these measurements will be given in order to support the assignments discussed in the preceding subsection and the validity of the application of the lattice-classification scheme (Fig. 1) presented in Sec. II.

Fe^{3+} (d^5). Recently, a structured near-infrared luminescence was attributed to the $^4T_1(G) \rightarrow {}^6A_1(S)$ emission of substitutional Fe^{3+} ions.[17] Besides the ZPL at 8177.3 cm^{-1} assigned to a cubic Fe^{3+} center at an AN site, some ZPL's shifted slightly to higher energies and some more strongly shifted lines have been observed. As in the case of Mn^{2+} centers, three centers with small energy shifts of +3.7, +9.2, and +12.7 cm^{-1} have been attributed to supplementary centers at impurity sites AN1, AN2, and AN3, respectively. (Among the other lines, only assignments to the sites PN, AS, and AS2 have been given.)

Co^{2+} (d^7). Within the absorption spectra due to the transition $^4A_2(F) \rightarrow {}^4T_2(F)$, in addition to the ZPL of the cubic center at 3523 cm^{-1}, additional ZPL's shifted to lower energy have been recorded.[18] Only the main centers connected to the sites AS, PN, and PS have been resolved, shifted by −18, −118, and −130 cm^{-1}. The authors presented a spectrum of a 4*H*-polytype crystal showing only the absorption due to Co^{2+} at an AS and a PN site with nearly equal absorption strength. This is in agreement with the expectation derived from the lattice classification.

The authors also determined the zero-field-splitting parameter D by EPR measurements and found the relation $D(\mathrm{AS}) + D(\mathrm{PN}) \approx D(\mathrm{PS})$. The same relation has been reported for Mn^{2+} EPR centers.[10]

Ni^{2+} (d^8). The absorption spectra connected to the transition $^3T_1(F) \rightarrow {}^3T_2(F)$ show the ZPL of the cubic center at 4383 cm^{-1}. Within a 6*H*-polytype crystal all main centers with nearly equal absorption have been observed.[19] The two axial centers were found to be shifted by −11 and −102 cm^{-1} and the hexagonal center by −113 cm^{-1}. From the lattice classification, the appearance of centers of the four different main sites are expected in the case of a 6*H*-polytype crystal, which contains ranges with different kinds of 6*H* structures.

Within transmission and emission spectra due to the transition $^3T_1(F) \leftrightarrow {}^3A_2(F)$, three polytype centers could be detected with comparable energy shifts.[20]

The examples summarized above provide strong support for the superposition principle and the validity of applying the lattice-classification scheme for the assignment of TM centers in stacking-faulted ZnS. Positive shifts of the SF centers with respect to the cubic center are found to appear if $dE/d\Delta < 0$, Δ being the crystal-

field parameter. Otherwise, negative shifts are observed. This is, of course, only a rough rule because, for example, the shifts observed within the Mn^{2+} $^4E(G)$ level cannot be described solely by the crystal-field model; see Sec. III A.

V. CONCLUSIONS

The optical transitions within the Mn^{2+} impurity in polymorphic ZnS have been used as a sensitive probe for the testing of the sequence of stacking layers within the microscopic range of six Zn-S double layers. Thus, a counterpart to the macroscopic Röntgen measurements has been presented. The energy shifts of the internal d^5 transitions induced by lattice distortions could be described by a superposition of the effects of specific faults within the lattice stacking order. A crystallographic classifiction scheme of the 16 impurity sites which are possible under consideration of the nearest and second-nearest neighborhood of the impurity has been given. On this bases, three new and nine known Mn^{2+} centers within excitation spectra to the $^4T_2(G)$ and $^4E(G)$ levels and the emission from the $^4T_1(G)$ level have been assigned to well-defined lattice sites. The validity of the superposition principle and of the application of the lattice classification for the assignments of stacking-faulted centers could also be demonstrated for other TM impurities in polymorphic or polytypic ZnS.

ACKNOWLEDGMENTS

The authors wish to thank H. Hartmann, Academy of Sciences (German Democratic Republic), for supplying some crystals and for performing Röntgen analysis. Also, the assistance of H.-J. Broschat, Technische Universität Berlin, for growing stacking-faulted samples, is appreciated.

[1]T. Buch, B. Clerjaud, B. Lambert, and P. Kovacs, Phys. Rev. B **7**, 184 (1973).
[2]D. Langer and S. Ibuik, Phys. Rev. **138**, A809 (1965).
[3]E. Neumann, thesis, Technische Universität Berlin, 1971.
[4]B. Lambert, T. Buch, and A. Geoffroy, Phys. Rev. B **8**, 863 (1973).
[5]W. Busse, H. -E. Gumlich, A. Geoffroy, and R. Parrot, Phys. Status Solidi B **93**, 591 (1979).
[6]U. W. Pohl, H. -E. Gumlich, and W. Busse, Phys. Status Solidi B **125**, 773 (1984).
[7]W. Busse, H. -E. Gumlich, W. Knaak, and J. Schulze, J. Phys. Soc. Jpn. Suppl A **49**, 581 (1980).
[8]R. Parrot, A. Geoffroy, C. Naud, W. Busse, and H. -E. Gumlich, Phys. Rev. B **23**, 5288 (1981).
[9]J. Schulze, thesis, Technische Universität Berlin, 1983.
[10]B. Clerjaud, B. Lambert, T. Buch, and R. Romestain, Phys. Lett. **42A**, 341 (1973).
[11]B. Di Bartolo, *Optical Interactions in Solids* (Wiley, New York, 1968).
[12]P. Koidl, Phys. Status Solidi B **74**, 477 (1976).
[13]C. Naud, thesis, Université Pierre et Marie Curie, 1982.
[14]R. Parrot, C. Naud, C. Porte, D. Fournier, A. C. Boccara, and J. C. Rivoal, Phys. Rev. B **17**, 1057 (1978).
[15]J. Schulze and H. -E. Gumlich, J. Cryst. Growth **59**, 347 (1982).
[16]R. Parrot and C. Blanchard, Phys. Rev. B **6**, 3992 (1972).
[17]A. Hoffman, R. Heitz, and I. Broser, Phys. Rev. B **41**, 5806 (1990).
[18]P. Koidl and A. Räuber, J. Phys. Chem. Solids **35**, 1061 (1974).
[19]U. Kaufmann, P. Koidl, and O. F. Schirmer, J. Phys. C **6**, 310 (1973).
[20]I. Broser, A. Hoffmann, R. Germer, R. Broser, and E. Birkicht, Phys. Rev. B **33**, 8196 (1986).